

Surface structure of the liquid Au₇₂Ge₂₈ eutectic phase: X-ray reflectivity

P. S. Pershan, S. E. Stoltz, and S. Mechler

Department of Physics and SEAS, Harvard University, Cambridge, Massachusetts 02138, USA

O. G. Shpyrko

Department of Physics, University of California–San Diego, San Diego, California 92093, USA

A. Y. Grigoriev

Department of Physics and Engineering Physics, The University of Tulsa, Tulsa, Oklahoma 74104, USA

V. S. K. Balagurusamy

Department of Physics, Brown University, Providence, Rhode Island 02912, USA

B. H. Lin and M. Meron

CARS, University of Chicago, Chicago, Illinois 60637, USA

(Received 28 April 2009; revised manuscript received 24 July 2009; published 16 September 2009)

The surface structure of the liquid phase of the Au₇₂Ge₂₈ eutectic alloy has been measured using resonant and nonresonant x-ray reflectivity and grazing incidence x-ray diffraction. In spite of the significant differences in the surface tension of liquid Ge and Au the Gibbs adsorption enhancement of Ge concentration at the surface is minimal. This is in striking contrast to all the other binary alloys with large differences in the respective surface tensions measured up to date. In addition there is no evidence of the anomalous strong surface layering or in-plane crystalline order that has been reported for the otherwise quite similar liquid Au₈₂Si₁₈ eutectic. Instead, the surface of eutectic Au₇₂Ge₂₈ is liquidlike and the layering can be explained by the distorted crystal model with only slight modifications to the first layer.

DOI: [10.1103/PhysRevB.80.125414](https://doi.org/10.1103/PhysRevB.80.125414)

PACS number(s): 68.03.Hj, 68.35.bd, 61.25.Mv

I. INTRODUCTION

The surface structure of liquid metals was essentially an unexplored phenomena until slightly more than a decade ago when the first synchrotron x-ray reflectivity studies on liquid metal surfaces were carried out.^{1,2} These measurements on liquid Hg (Ref. 1) and Ga (Ref. 2) confirmed the proposal by Rice and colleagues^{3–5} that the local order at the free surface was sufficient to induce atomic layering. This layering decays within a distance from the surface of the order of the bulk liquid correlation length, i.e., 3–4 atomic layers.^{4,5} The layering is observed as a peak in the specular reflectivity at the wave vector transfer vector $q_z = 2\pi/d$ where d is the layering distance. Subsequent studies on liquid In,⁶ K,⁷ Sn,⁸ and Bi (Ref. 9) revealed a similar type of layering at the surface of these liquids, demonstrating that this phenomenon appears to be universal for metallic liquids, regardless of the surface tension, i.e., $\gamma = 110$ mN/m for K, 560 mN/m for Sn, and 770 mN/m for Ga.

Furthermore, similar studies that have been carried out on various liquid metal alloys; i.e., In₇₈Bi₂₂,¹⁰ Sn₅₇Bi₄₃,¹¹ Ga_{83.5}In_{16.5},¹² as well as on Ga- or Hg-based dilute alloys Ga-Bi,^{13,14} Ga-Pb,¹⁵ Ga-Tl,¹⁶ Hg-Au (Ref. 17) have all demonstrated Gibbs adsorption effects by which the top surface layer is enriched in the respective element with the lower surface tension. The only exceptions for which Gibbs adsorption has not been observed is an alloy of otherwise very similar elements, K₆₇Na₃₃.¹⁸ Although for all these alloys the surface enriched layer in principle is liquidlike, Rice observed that on approaching the liquidus coexistence line the fluidlike monolayers of both Tl and Pb at the surface of the

Ga-rich Ga-Pb (Ref. 15) and Ga-Tl (Ref. 16) alloys form two-dimensional (2D) crystals with a lattice structure that is different from that of the bulk phase.

The surface order that appears over a wider range of temperatures above the eutectic temperature of the Au₈₂Si₁₈ eutectic is yet a very different phenomenon.^{19,20} The first, and most amazing empirical effect for the Au₈₂Si₁₈ liquid is the anomalously strong surface layering that is revealed by a reflectivity peak which is more than an order of magnitude more intense than for any of the other metals or alloys that have been studied. Furthermore grazing incidence diffraction studies demonstrated that the anomalously strong reflectivity is accompanied by a 2D crystalline bilayer surface phase²¹ with an in-plane rectangular (AuSi₂) unit-cell structure. On heating about 12 K above the melting temperature this anomalously strong reflectivity decreases via a first order transition to a weaker, but still enhanced reflectivity and the bilayer structure transforms into a 2D crystalline monolayer. The effect is reversible on cooling. There are no known stable intermetallic Au-Si phases that resemble the lattice constants for the 2D AuSi₂ phase; however, there are similarities to phases that have been observed in thin metastable solid Au-Si films.^{22–24}

At the present time there is no theoretical explanation for the Au-Si surface effect; however, it is reasonable to speculate that it might arise from the relatively strong covalency between Au and Si. In the absence of reliable theoretical guidance it is natural to ask whether the Au-Ge system exhibits a surface structure that is similar to that found in Au-Si. As shown in Fig. 1 the phase diagram of Au-Ge exhibits a deep eutectic that is similar to the Au-Si system and with a

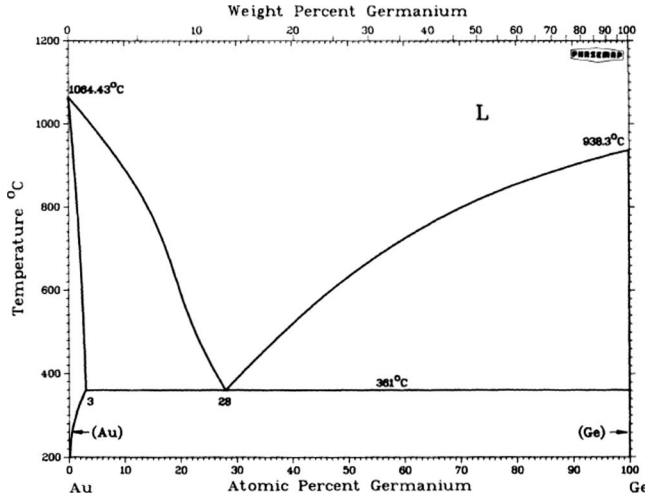


FIG. 1. Phase diagram of Au-Ge (Ref. 27) showing a simple eutectic at a composition at Au₇₂Ge₂₈ and a low eutectic temperature of 634 K as it is also known for the Au-Si system. With kind permission of Springer Science and Business Media.

eutectic temperature that is essentially the same. Just as in Au-Si there are no known stable intermetallic phases and the solubility of Ge in Au and vice versa in the solid state is low. Aside from the fact that Au-Ge (Ref. 25) does not form the same kind of amorphous phase on rapid quenching of the liquid phase as Au-Si (Ref. 26) the two systems seem otherwise alike.

We report experiments here that reveal that the surface order of the liquid Au₇₂Ge₂₈ eutectic shows no evidence of the anomalous surface-induced order that has been observed for the Au₈₂Si₁₈ eutectic. Furthermore, there is no evidence for Gibbs adsorption found in other binary liquid metal alloys with such dissimilar components.

II. BACKGROUND

The kinematics of x-ray scattering from liquid surfaces has been discussed in a number of recent papers.^{7,28-30} X-rays of wavelength λ are incident on the xy plane of the liquid surface at an angle α . The scattered radiation is detected by a rectangular slit of horizontal and vertical widths ($h \times w$) at a distance L from the sample. The detector slit is located at an angle β to the xy surface in a plane that makes an angle θ to the plane of incidence. For a typical modern synchrotron x-ray reflectivity experiment, we can neglect the x-ray beam divergence, the energy resolution, and the width of the incident beam in respect to the size of the detector slits. The angular resolution are $\Delta\theta = w/L$ and $\Delta\beta = (h/L)\cos\beta$. The three components of the wave vector transfer for radiation striking the center of the detector are

$$\begin{aligned} q_x &= (2\pi/\lambda)\cos\beta\sin\theta \\ q_y &= -(2\pi/\lambda)(\cos\alpha - \cos\beta\cos\theta) \\ q_z &= (2\pi/\lambda)(\sin\alpha + \sin\beta) \end{aligned} \quad (1)$$

It has been shown^{7,31} that the equation which describes the specular reflectivity from a liquid metal surface can be broken up into three terms

$$R(q_z) = R_F(q_z) \times CW(q_z) \times |\Phi(q_z)|^2. \quad (2)$$

The first term, R_F , is the theoretical Fresnel x-ray reflectivity from an abrupt flat interface between vacuum and the bulk. For $q_z \gg q_c$ (≈ 5 times larger) $R_F(q_z)$ has the simple form of:

$$R_F(q_z) \approx \left(\frac{q_c}{2q_z}\right)^4. \quad (3)$$

For an incident angle α which corresponds to q_z smaller than the critical wave vector q_c the x-rays are fully reflected. We have used a more complete expression for $R_F(q_z)$ that also includes x-ray absorption but the results are indistinguishable. The critical wave-vector q_c is given by $q_c = 4\sqrt{\rho_\infty r_0 \pi}$ where ρ_∞ is the effective bulk electron density, which includes the resonant reduction in scattering amplitude, and r_0 is the classical electron radius of 2.818×10^{-5} Å. When presenting reflectivity data, which typically ranges over ~ 10 orders of magnitude, it is convenient to divide the data by $R_F(q_z)$.

The second term in Eq. (2), $CW(q_z)$, is a Debye-Waller-like factor due to thermally excited capillary waves, which depends on the temperature, T , and the surface tension, γ .

$$CW(q_z) = \int_{A_{q_{xy}}} d^2q_{xy} \left(\frac{q_{xy}}{q_{\max}}\right)^\eta \frac{\eta}{2\pi q_{xy}^2} \quad (4)$$

where $\eta = \frac{k_B T}{2\pi\gamma} q_z^2$, q_{\max} is the cut-off wavevector of the system (here 1.45 \AA^{-1}) and $A_{q_{xy}}$ is the projection of the detector slit in q space.³² Note that the value of the integral depends on the experimental resolution. The acceptance angle of the detector slit is: $\Omega = \Delta\theta \times \Delta\beta \times \cos(\beta)$.

Dividing the experimental data by both $R_F(q_z)$, (which only depends on the bulk electron density) and $CW(q_z)$ (which is accurately known from capillary wave theory) one obtains the surface structure factor $|\Phi(q_z)|^2$ where $\Phi(q_z)$ itself only depends on the electron-density profile along the surface normal.

$$\Phi(q_z) = \frac{1}{\rho_\infty} \int dz \frac{d\langle\rho(z)\rangle}{dz} \exp[iq_z z]. \quad (5)$$

Here $\langle\rho(z)\rangle$ denotes the surface parallel average of the surface electron density at a position z along the normal to the surface and ρ_∞ is the electron density in the bulk liquid. The electron density $\langle\rho(z)\rangle$ is generally obtained by numerical fitting of the measured reflectivity, $R(q_z)$, divided by $R_F(q_z)$ and $CW(q_z)$ with the physical model described below.

A simple but very useful model for the electron density in liquid metals is derived from a version of the distorted crystal model (DCM),¹ in which the ratio of the average atomic density at some position z along the surface normal in the bulk liquid is described by a sum of GAUSSIAN functions separated by a distance, d

$$\frac{\langle\rho_{DCM}^a(z)\rangle}{\rho_\infty^a} = \sum_{n=0}^{\infty} \frac{d}{\sigma_n \sqrt{2\pi}} \exp\left[-\frac{(z-nd)^2}{2\sigma_n^2}\right]. \quad (6)$$

In this model the width of the GAUSSIAN functions increases with the distance from the surface, $\sigma_n^2 = \sigma_0^2 + n\bar{\sigma}^2$. As the distance from the surface increases the model approaches a uniform function whose value is just unity. The superscript *a* refers to atomic densities. Substitution (of $\langle \rho_{DCM}^a(z) \rangle / \rho_\infty^a$) into Eq. (5) obtains the very convenient analytic expression for the atomic analog of the structure factor.

$$\begin{aligned} \Phi_{DCM}^a(q_z) &= iq_z d \sum_{n=0}^{\infty} \exp[iq_z dn] \exp[-q_z^2 \sigma_n^2 / 2] \\ &= iq_z d \frac{\exp[-\sigma_0^2 q_z^2 / 2]}{1 - \exp[iq_z d] \exp[\bar{\sigma}^2 q_z^2 / 2]}. \end{aligned} \quad (7)$$

Despite having only three parameters the surface structure factor that is obtained by convolution of $\Phi_{DCM}^a(q_z)$ with the atomic form factors describe the reflectivity from Ga, In, and K exceptionally well. The surface structure of others such as Sn and Bi can only be described with slight modifications of the DCM and we will show below that similar modifications of the DCM are necessary for Au₇₂Ge₂₈.

The simplest atomic density model that will adequately describe the Au-Ge data requires modification of the topmost atomic layer at the liquid/vapor surface. Although this can be done in different ways the most convenient is to supplement the DCM by addition of an adlayer between the vapor and the DCM. The atomic distribution of this layer can be described by three additional parameters: its integrated density N_A , its position P_A and width σ_A

$$\frac{\langle \rho_A^a(z) \rangle}{\rho_\infty^a} = \frac{N_A d}{\sigma_A \sqrt{2\pi}} \exp\left[-\frac{(z - P_A)^2}{2\sigma_A^2}\right] \quad (8)$$

where the factor N_A , which specifies the integrated atomic density of the adlayer, is expressed in terms of the atomic volumes (V_{Ge} , V_{Au}) of Ge and Au and their surface and bulk concentrations (X_A and X_∞)

$$N_A = \frac{X_\infty V_{Au} + (1 - X_\infty) V_{Ge}}{X_A V_{Au} + (1 - X_A) V_{Ge}}. \quad (9)$$

The resulting bulk normalized electron density has the form

$$\begin{aligned} \frac{\langle \rho(z) \rangle}{\rho_\infty} &= \frac{\langle \rho_A^a(z) \rangle}{\rho_\infty^a} \otimes \frac{X_A F_{Au}(z) + (1 - X_A) F_{Ge}(z)}{X_\infty Z_{Au} + (1 - X_\infty) Z_{Ge}} \\ &+ \frac{\langle \rho_{DCM}^a(z) \rangle}{\rho_\infty^a} \otimes \frac{X_\infty F_{Au}(z) + (1 - X_\infty) F_{Ge}(z)}{X_\infty Z_{Au} + (1 - X_\infty) Z_{Ge}} \end{aligned} \quad (10)$$

where \otimes denotes convolution and $F_{Au}(z)$ and $F_{Ge}(z)$ is the *xy* integral of the atomic electron-density distributions for Au and Ge, respectively. If the energy dispersive effects are neglected, atomic form factors $f(q_z)$ are just the Fourier transforms of the electron densities, $f(q_z) = \int dz F(z) \exp[iq_z z]$ [note that $f(0) = Z$]. As a practical matter we use tabulated values of the form factor.³³ If energy dispersive effects were negligible the surface structure factor could be modeled by substitution of Eq. (10) into Eq. (5)

$$\begin{aligned} \Phi(q_z) &= \Phi_A^a(q_z) \frac{X_A f_{Au}(q_z) + (1 - X_A) f_{Ge}(q_z)}{X_\infty f_{Au}(0) + (1 - X_\infty) f_{Ge}(0)} \\ &+ \Phi_{DCM}^a(q_z) \frac{X_\infty f_{Au}(q_z) + (1 - X_\infty) f_{Ge}(q_z)}{X_\infty f_{Au}(0) + (1 - X_\infty) f_{Ge}(0)}. \end{aligned} \quad (11)$$

The contribution from the DCM, $\Phi_{DCM}^a(q_z)$, is given in Eq. (7) and the contribution from the adlayer $\Phi_A^a(q_z)$ is

$$\Phi_A^a(q_z) = iq_z N_A d \exp[iq_z P_A] \exp[-q_z^2 \sigma_A^2 / 2]. \quad (12)$$

The effect of energy dispersion can be taken into account by recognizing that for near forward scattering the effective number of electrons for a Z-electron atom varies as $Z_{eff} = Z + f'_{q_z=0}(E)$ where $f'_{q_z=0}(E)$ is the energy dependent correction to the atomic scattering amplitude.³⁴

The effect that is used here to probe the difference between the Ge surface and bulk concentrations is based on the fact that close to an absorption edge $f'_{q_z=0}(E)$ becomes a significant negative number. For an alloy the energy dependent change in contrast between surface and bulk can be used to determine if surface segregation occurs. We approximate the energy dependent form factor $f(q_z, E)$ as

$$f(q_z, E) = f(q_z) \frac{Z + f'_{q_z=0}(E)}{Z} \quad (13)$$

where tabulated values are used for the energy dependent correction $f'_{q_z=0}(E)$.³⁴ The compound form factor for an Au_xGe_{1-x} alloy is not known and as a practical matter we approximate the total expression for $\Phi(q_z, E)$ in our model as

$$\begin{aligned} \Phi(q_z, E) &= \Phi_A^a(q_z) \frac{X_A f_{Au}(q_z, E) + (1 - X_A) f_{Ge}(q_z, E)}{X_\infty f_{Au}(0, E) + (1 - X_\infty) f_{Ge}(0, E)} \\ &+ \Phi_{DCM}^a(q_z) \frac{X_\infty f_{Au}(q_z, E) + (1 - X_\infty) f_{Ge}(q_z, E)}{X_\infty f_{Au}(0, E) + (1 - X_\infty) f_{Ge}(0, E)}. \end{aligned} \quad (14)$$

This model has six adjustable parameters (d , σ_0 , $\bar{\sigma}$, P_A , σ_A , and X_A). The first three parameters: d , σ_0 , and $\bar{\sigma}$ give the DCM part of the model, where d is the distance between layers, σ_0 is the width of the first layer, and the $\bar{\sigma}$ parameter determines the increase in width for subsequent layers. The surface structure factor obtained with only the DCM model, $|\Phi_{DCM}^a(q_z)|^2$ is a monotonic increasing function from unity at $q_z = 0$ to a peak located at $\sim 2\pi/d$. The peak width is determined by $\bar{\sigma}$ and its height originates from both σ_0 and $\bar{\sigma}$.

The last three parameters refers to the adlayer: σ_A , P_A , and X_A define the width, the position, and the atomic Au concentration. These parameters can be chosen so that the adlayer becomes a part of the DCM, i.e., $\sigma_A = \sqrt{\sigma_0^2 - \bar{\sigma}^2}$, $P_A = -d$, and $X_A = X_\infty$. If the parameters depart from these values the interference between the layers in the model is altered and the structure factor can exhibit structure that deviates from the monotonically increasing behavior of the DCM.⁹

The effective bulk electron density ρ_∞ that we later use to set the critical angle for total reflection, q_c , of the liquid Au-Ge sample is given by

TABLE I. Dispersive corrections to the atomic scattering amplitudes $f'_{q_z=0}(E)$ for Au and Ge at different x-ray energies, used to model the measured reflectivities using Eq. (14).

	11.05keV	11.915keV	12.00keV
$f'_{Ge}(E)$	-4.8	-1.7	-1.6
$f'_{Au}(E)$	-7.5	-17.6	-12.0

$$\rho_\infty = \frac{X_\infty[Z_{Au} + f'_{Au}(E)] + (1 - X_\infty)[Z_{Ge} + f'_{Ge}(E)]}{X_\infty V_{Au} + (1 - X_\infty)V_{Ge}} \quad (15)$$

An alternative way to construct a model with a DCM plus one layer would be to substitute/exchange the outermost layer in the DCM model instead of adding another layer. If $\bar{\sigma}_0 < \sigma_0$ it is easy to show that by adjusting σ_0 this model can be made equivalent to the adlayer model.

III. EXPERIMENTAL

The Au-Ge sample material was obtained from Goodfellow Inc. as commercially available high purity Au₇₂Ge₂₈ eutectic alloy (99.97% metals basis). The alloy was melted inside an ultrahigh vacuum x-ray chamber in a molybdenum pan that is heated by an boralelectric heater from the bottom side. A K-type thermocouple was directly mounted to the side of the molybdenum pan to measure the temperature of the sample.

After initial melting of the alloy some germanium oxide patches remained on the surfaces. These have been removed at first by mechanically scraping/wiping the surface with a molybdenum scraper. Remaining oxide particles were then eliminated from the surface by Ar⁺ ion beam sputtering at 5 keV for several hours. The liquid surface then was free of any visible oxide. Further proof that the surface was clean is the observation that the x-ray reflectivity was unchanged when the beam was translated across the sample. The sample was kept at a temperature of about 5–10 K above the eutectic temperature of 637 K. During reflectivity measurements the vacuum was in the 10⁻⁹ mbar range.

The x-ray measurements have been performed using the liquid reflectometer at the beamline ID-15 at ChemMat-CARS, Advanced Photon Source at Argonne National Laboratory. X-ray reflectivity (XR) studies were carried out at 11.050 keV, i.e., slightly below the K-absorption edge of Ge at 11.103 keV, at 11.915 keV that is slightly below the L3-absorption edge of Au at 11.919 keV, as well as at 12.000 keV. The corresponding corrections to the atomic scattering amplitudes used to analyze the reflectivity data are summarized in Table I. The atomic scattering amplitudes were taken from analytical approximation to the scattering factor tables in Ref. 34.

For the reflectivity studies vertical soller slits were mounted in front of the scintillation counter point detector. The horizontal angular resolution of the soller slits is 2.0 mrad. Additionally a vertical slit of 6 mm height in a distance of 685 mm from the sample gives a vertical resolution of 7.0 mrad. Complementary grazing incidence x-ray diffrac-

tion (GIXRD) has been performed using the soller slits with the same angular resolution, but the vertical slits were set to 10 mm.

Although the critical angle for total reflection, q_c , of the liquid Au-Ge sample could not be measured reliably due to a rather small curvature of the liquid sample of about 1200 mm the value of q_c could be calculated from the effective electron density of the Au-Ge liquid, ρ , by Eq. (1) using the equation for q_c that was given following Eq. (3). The atomic volumes V_{Au} and V_{Ge} were calculated by a hexagonal close packed sphere approximation using a radius of Au of 1.44 Å and of Ge of 1.22 Å. This implies a substitutional occupancy of Au and Ge in the structure of liquid Au₇₂Ge₂₈, as it was deduced from the bulk structure factor for liquid Au₇₂Ge₂₈, and also for liquid Au₈₂Si₁₈.^{35,36} The values of q_c were found to be 0.0745 Å⁻¹, 0.0703 Å⁻¹, and 0.073 Å⁻¹ for x-ray energies of 11.05, 11.915 and 12.00 keV, respectively. By a similar calculation for Au₈₂Si₁₈, for which q_c is precisely known,²¹ we estimated the error for this method to be around 4%.

IV. RESULTS

The measured reflectivity curves for liquid Au₇₂Ge₂₈ taken at a sample temperature at 647 K, i.e., 10 K above the eutectic temperature and at x-ray energies of 11.05, 11.915, and 12.00 keV are shown in Fig. 2(a). The reflectivity curves correspond to the difference between the signal observed in the plane of incidence and signals measured at ±0.15 degree to either side of the plane of incidence. The solid line in the figure illustrates the theoretical $R_F(q_z)$ for the data taken at 11.05 keV, for which $q_c=0.0745$ Å⁻¹. In view of the fact that the R_F curves of the other energies only differ by less than ~2.5% they would be indistinguishable from each other on this plot. Clearly, the reflectivity data measured at different energies do not differ significantly from each other at q_z less than 2.2 Å⁻¹. The differences at larger q_z arise from statistical errors due to the combination of the very low intensity of the reflected beam and the strongly increasing background scattering from the bulk Au-Ge liquid. The reflectivity curve measured at 11.05 keV was normalized to the direct beam. The data for the 11.915 and 12.00 keV reflectivity curves were normalized to the 11.05 keV data in the small q_z region. The experimentally determined q_c for 11.05 keV of 0.0745 Å⁻¹ agree with the previously obtained using a hard sphere model.

In order to better visualize the data the ratio $R(q_z)/R_F(q_z)$ for the different energies is shown in Fig. 2(b). Here the shape of the reflectivities, i.e., the noticeable increase in slope around $q_z=1.7$ Å⁻¹ is clear proof of surface layering^{7,37} of the Au₇₂Ge₂₈ liquid. Added in the figure is the theoretical form for $CW(q_z)$ which itself is a known function of the surface tension. As discussed elsewhere^{6–8,37} the surface tension can be determined from the off-specular diffuse scattering as it is shown in Fig. 3 for the Au-Ge liquid measured with a x-ray energy of 11.05 keV at incidence angle, α , of 5.15 degree that corresponds to $q_z=1$ Å⁻¹. The algebraic singularity is best measured with the highest possible resolution. On the other hand, if the slit is too small (resolution

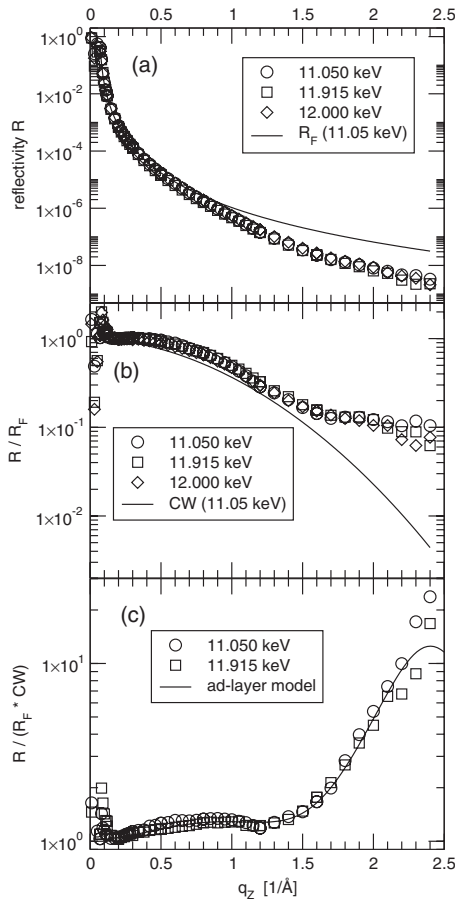


FIG. 2. (a) X-ray reflectivity of eutectic Au₇₂Ge₂₈ measured at x-ray energies of 11.05, 11.915 and 12.00 keV. Additionally the Fresnel reflectivity curve (R_F) is plotted that was obtained by fitting the reflectivity at 11.05 keV in the low q_z range. (b) Reflectivity of liquid Au₇₂Ge₂₈ after normalization by the respective Fresnel reflectivity, i.e., R/R_F . Added is the contribution of capillary wave function, $CW(q_z)$, to the reflectivity at 11.05 keV. (c) The same data after normalization by the respective R_F and the contribution from capillary waves, CW , i.e., $R/(R_F * CW)$. The solid line represents the best fit to the data using the adlayer model as given by Eq. (10).

too high) it would become necessary to account for the angular divergence of the incident beam and the effects of the sample curvature. The diffuse data is best analyzed by choosing a slit height that produces the flat top shown and then comparing the data with the integral of the algebraic singularity over the known resolution. The various lines through the data correspond to different values of the surface tension, γ , used in Eq. (4). The data is best represented by a surface tension of 867 mN/m which is the value obtained by the best NLLS (nonlinear least square) fit. The broken lines illustrate calculated diffuse scattering for $\eta=667$ mN/m and 1067 mN/m and are included to give an idea about the sensitivity of γ as fitted parameter. We determine the surface tension to be 867 ± 100 mN/m and we use the value 867 mN/m in calculating the $CW(q_z)$, that is plotted as the solid line in Fig. 2(b).

Figure 2(c) shows the experimental data obtained at 11.050 and 11.915 keV after division with $R_F(q_z)$ and $CW(q_z)$. This data can now be compared directly with the

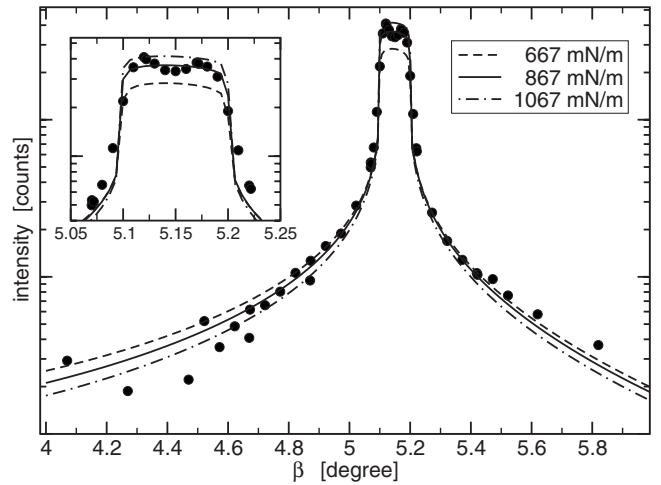


FIG. 3. Off-specular diffuse scattering measured with a x-ray energy of 11.05 keV at incidence angle, α , of 5.15 degree. The dots, •, represent data points and the lines represents calculated off-specular diffuse scattering for different surface tensions. The solid line ($\gamma=867$ mN/m) shows the best fit. The broken lines at ± 200 mN/m are included to give an idea about the sensitivity of fitted parameter γ .

surface structure factor, $|\Phi(q_z)|^2$. The data exhibits two prominent features. The first is the broad maximum centered around $q_z=0.8 \text{ \AA}^{-1}$. The second is the steep rise for q_z higher than 1.5 \AA^{-1} that originates from surface layering.^{7,37} On the other hand, because of the first broad first maximum (or in other words the occurrence of the minimum at around $q_z=1.2 \text{ \AA}^{-1}$) slight modifications to the first layer are needed, as the DCM produces a monotonically increasing structure factor in this range.

Although a similar effect, i.e., a local minimum in the surface structure factor was also observed for elemental Sn (Ref. 8) and Bi (Ref. 9) the origin in this binary alloy can be different since here in Au-Ge there is the possibility that as a consequence of Gibbs adsorption the chemical composition of the first layer(s) could be different from the bulk.^{11,30,38} The fact that the structure factor data at 11.915 and 11.05 keV are virtually identical would seem to imply that this is not the case, nevertheless, the following analysis is directed toward just this issue. To account for the minimum in the structure factor the electron-density model has to be adjusted in a similar manner as it was necessary for the surface of liquid Sn (Ref. 8) and Bi (Ref. 9) by introduction of a top surface adlayer with a width and a distance to the next layer that is different from requirements of the DCM.

The solid line in Fig. 2(c) displays the result of a simultaneous fit of both the 11.05 and 11.915 keV experimental data to the respective surface structure factor using the ad-layer model given by Eq. (14) and a surface concentration of Ge(1- X_A) of 28 at. % that is identical to the bulk value. The energy dispersion was accounted for using the values for the dispersive corrections to the real part of the atomic scattering amplitudes that are given in Table I. In view of the fact that the surface structure factor is independent of energy the concentrations in the adlayer and bulk are the same. Although the critical angle is energy dependent this only affects $R_F(q_z)$

TABLE II. Parameters for the adlayer and DCM models obtained by NLLS fit of the 11.05 and 11.915 keV data with Eq. (14). Parameters are explained in the background section. Note that the Ge concentration in the adlayer is $1-X_A$.

	σ_0 (Å)	$\bar{\sigma}$ (Å)	d (Å)	X_A	σ_A (Å)	P_A (Å)
Adlayer (28 at. % Ge)	0.71	0.58	2.5	0.72	0.60	-2.43
Adlayer (50 at. % Ge)	0.74	0.64	2.5	0.50	0.54	-2.38
Adlayer (75 at. % Ge)	0.78	0.75	2.5	0.25	0.46	-2.30
Adlayer ($d=2.4$ Å)	0.67	0.64	2.4	0.72	0.55	-2.35
Adlayer ($d=2.6$ Å)	0.76	0.53	2.6	0.72	0.65	-2.52

that does not affect the prediction for $R(q_z)/[R_F(q_z) \times CW(q_z)]$ that is represented by the single solid line in Fig. 2(c). The model parameters are given in the first row in Table II and the corresponding electron density profile is represented by the solid line in Fig. 4.

To illustrate the effect of a varying concentration of Ge in the adlayer, the structure factors for both energies (11.050 and 11.915 keV) were again fitted simultaneously for fixed surface concentrations of Ge of 50 and 75 at. %, respectively [see Fig. 5(a)]. It is evident from these best possible fits that even a modest surface enrichment of Ge to 50 at. % leads to a spreading of the respective structure factors, which is not represented by the data. The structure factors for 75 at. % Ge surface concentration are even more different, indicating that indeed the surface enrichment of Ge in $Au_{72}Ge_{28}$ is not very significant. The parameters for these fits for 50 and 75 at. % Ge are shown in the second and third row in Table II.

As previously mentioned, because of the minimum centered around $q_z \approx 1.2 \text{ \AA}^{-1}$ it is theoretically impossible to fit the data with only the DCM. One way to demonstrate the inadequacy of the DCM in fitting this data is illustrated by the electron-density profile illustrated by the broken line in Fig. 4. This model is constructed by constraining the width, position, and amplitude of the adlayer to be precisely what it

would be if the DCM was extended to the surface. As can be seen the effect is that in this model peak amplitude of the first layer is about 1/3 larger than the best fit adlayer model. The effect on the structure factor is illustrated with the broken line in Fig. 5(b). Furthermore, the dotted line in Fig. 5(b) illustrates the structure factor for a DCM in which the value

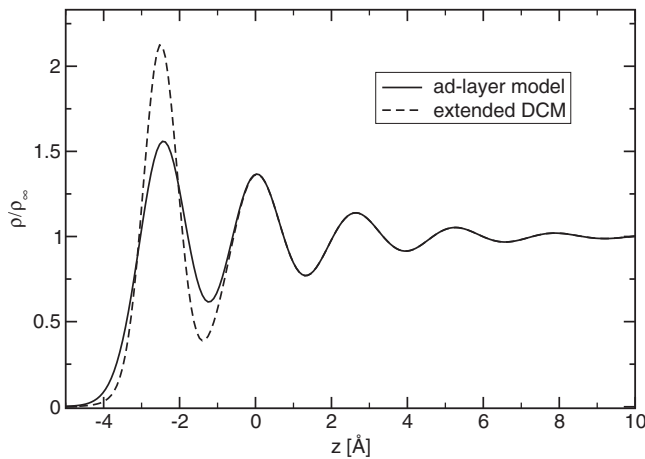


FIG. 4. The solid line denotes the electron density profile of the best fit using the adlayer model. The broken line shows the electron density profile when the parameters for the DCM are extended to the adlayer.

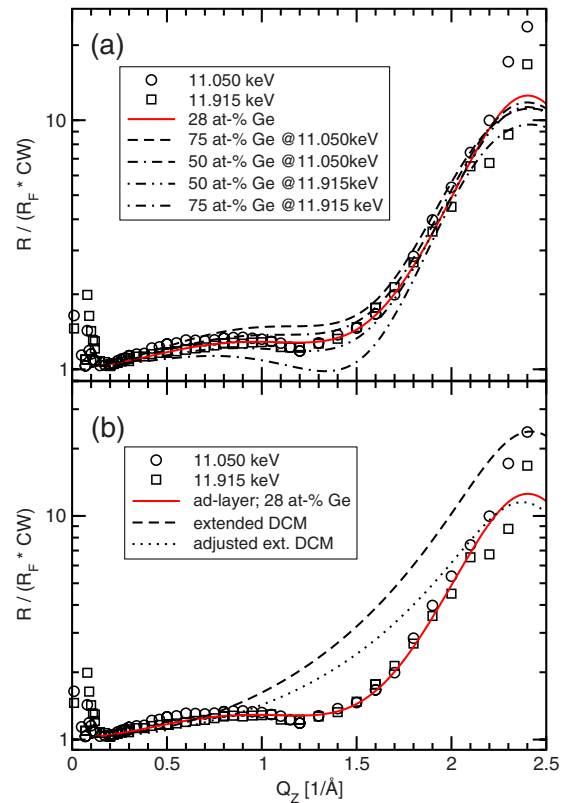


FIG. 5. (Color online) (a) The lines represent the surface structure factor of liquid $Au_{72}Ge_{28}$ as calculated for x-ray energies of 11.05 and 11.915 keV. The solid red line denotes the best fit to the data using the adlayer model as given by Eq. (10). Here the Ge concentration in the adlayer is the same as in the bulk. The broken lines represent theoretical modeling of the surface structure factor using a Ge concentration in the adlayer different from the bulk. (b) Again the solid red line denotes the best fit to the data using the adlayer model. The broken line is the structure factor from the electron density shown as a broken line in Fig. 4. The dotted line is obtained by increasing σ_0 from 0.41 \AA to 0.55 \AA to better match the height of the peak.

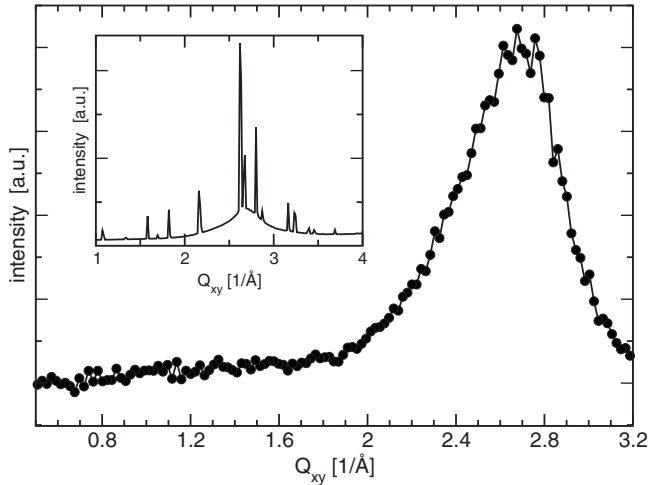


FIG. 6. Grazing incidence x-ray diffractogram of the surface of liquid Au₇₂Ge₂₈ and Au₈₂Si₁₈ slightly above the eutectic temperature. The Au₇₂Ge₂₈ surface does not produce discrete Bragg reflections like those found in the Au₈₂Si₁₈ liquid (see inset) but only the diffuse diffraction maxima that characterizes a liquid surface.

of σ_0 were chosen (increased) to match the peak amplitude of the structure factor. These traces illustrate that even slight changes in the relation between the first and subsequent layers in the DCM are sufficient to destroy the subtle interference that gives rise to the monotonically rising low q_z structure factor. In the best-fit model the broad low q_z maxima and subsequent minima at $q_z \approx 1.2 \text{ \AA}^{-1}$ were the consequence of slight broadening and shifting of the first layer.

On the other hand, as was seen in other systems^{8,9,19,20} for the modified DCM with the adlayer the parameters are considerably crosscorrelated and it is possible also for Au₇₂Ge₂₈ to get fits that are essentially as good with a layering spacing parameter, d , that are constrained to be different from 2.5 Å those in Table II. For example, the last two rows in Table II display the best-fit parameters if the layer spacing is constrained to be either 2.4 Å or 2.6 Å rather than 2.5 Å. A significantly larger value, say 2.65 Å, is unacceptable in that it causes the surface layering peak to move to a value of q_z that is clearly too small. On the other hand values of layer spacing that are much smaller, say 2.35 Å are not consistent with the close packed spheres with the covalent radius of Au (1.44 Å).

Although the absence of a strong enhanced peak in the reflectivity does strongly suggest the absence of crystalline 2D surface order such as that found for Au₈₂Si₁₈, the data for the GIXRD measurement shown in Fig. 6 indicates this directly. The GIXRD data were measured at an incidence angle of about 4.1 mrad that is well below the critical angle (5.8 mrad). Clearly, there is no sign of sharp Bragg reflections found at the surface of liquid Au₈₂Si₁₈ eutectic (see inset in Fig. 6). Nevertheless, due to the small radius of curvature of the liquid Au₇₂Si₂₈ sample it is possible that some portion of the x-rays has a higher incidence angle above the critical angle and should therefore penetrate into the bulk liquid. For a beam height of 0.02 mm, the illuminated area of the sample is <7 mm at an incident angle relative to the horizontal of $\alpha=0.18^\circ$. For the radius of curvature of 1200 mm, the varia-

TABLE III. Comparison of physical parameters for eutectic Au-Si and Au-Ge alloy. x_{bulk} is the concentration of the respective solute, ΔH_{mix} the atomic mixing enthalpy according to Ref. 39 T_m the respective eutectic temperatures and γ the surface tension of the pure liquid phase of Si and Ge.⁴⁰

	Units	Si	Ge
x_{bulk}	(at. %)	18	28
$\Delta H_{\text{mix}}(\text{Au-X})$	(kJ/mol)	-30	-21.5
T_m (eutectic)	(K)	637	637
γ	(mN/m)	865	621

tion in the angle of the x-ray beam with the liquid surface is $< \pm 0.5 \times (7/1200) \text{ rad} \approx 0.17^\circ$ implying a range for the angle of incidence relative to the local surface from 0.01 to 0.35 degree. For this range of angles, the penetration into the bulk cannot be more than a few tens of Ångströms. In view of the fact that the Bragg reflections in liquid Au₈₂Si₁₈ can also still be detected when the incidence angle is above the critical angle, although with lower intensity relative to the bulk scattering, the absence of observable Bragg peaks for Au₇₂Ge₂₈ does strongly suggest the absence of 2D crystalline surface order. The broad maximum centered around $q_{xy} = 2.65 \text{ \AA}^{-1}$ that is characteristic of the bulk liquid structure factor and that is similar to published data for the bulk liquid^{35,36} is the only feature of this data, indicating that the surface of liquid Au₇₂Ge₂₈ is liquidlike.

V. DISCUSSION

The principal result from this study is the demonstration that the surface structure of the liquid Au₇₂Ge₂₈ eutectic does not exhibit the same extraordinary properties that were found recently for liquid eutectic Au₈₂Si₁₈, i.e., a strong layering normal to the surface that is accompanied by an in-plane 2D crystalline long-range order. The liquid phase of Au-Ge only shows a modest, standardlike surface layering that is similar to the majority of the metallic liquids investigated so far. The broad low q_z structure of the Au-Ge alloy is qualitatively similar to what was found for elemental Sn and Bi. It is not really clear whether the subtle layer structure of the DCM that predicts smoothly monotonic low q_z growth in the structure factor for Ga, In, and K should be more remarkable than the first layer deviations that give rise to in the properties of Sn, Bi, and Au-Ge. These are clearly issues that call out for theoretical guidance.

From one point of view the difference between Au-Ge and liquid Au-Si is somewhat surprising in that the phase diagram and the physical parameters for Ge and Si are so similar. Their mixing enthalpy with Au, the surface tension of the pure element and the eutectic temperature, that are given in Table III are not dramatically different. The first experimental observation that would appear to correlate with the absence of the surface anomaly for Au₇₂Ge₂₈ is the measurement of the temperature dependence of ion emissivity from eutectic Au-Ge and Au-Si liquid surfaces.^{41,42} According to these measurements the temperature derivative of the surface

tension just above the melting point is positive for the $\text{Au}_{82}\text{Si}_{18}$ and negative for $\text{Au}_{72}\text{Ge}_{28}$. In view of the fact that the sign of the derivative should be determined by the degree of surface order⁴³ these results imply that the $\text{Au}_{72}\text{Ge}_{28}$ surface should be more disordered than that of $\text{Au}_{82}\text{Si}_{18}$ which is in accordance to the measurements presented here. On the other hand, this belies the point since we do not understand why it should be so.

At some level the difference between the surface properties of liquid $\text{Au}_{82}\text{Si}_{18}$ and $\text{Au}_{72}\text{Ge}_{28}$ probably has to be related to the kind of short-range order present in the bulk liquid phase, i.e., to the chemical interactions between Au and Si and on the other hand between Au and Ge. One property that might be important when discussing the origin of crystalline surface phases in metallic liquid alloys is the glass forming ability of the respective alloy. Interestingly, liquid alloys of Au-Si at composition around the eutectic can be cast into the amorphous phase by rapid quenching technologies,²⁶ while for Au-Ge it only produces metastable intermetallic phases.²⁵

It is known that glass forming liquids have a rather high degree of short-range order in the liquid as well as in the undercooled liquid.^{44,45} It is possible that the relatively small difference between the enthalpy of mixing, which for Au-Si is approximately 30% larger than for Au-Ge, is sufficient to account for the different properties; however, this would seem surprising. Interestingly, all other liquid metallic binary alloys investigated so far such as, for example, Au-Sn, In-Bi, and Sn-Bi show a much smaller enthalpy of mixing than both Au-Si and Au-Ge and in some cases the enthalpy of mixing is nearly zero (as is the case for In-Bi and Sn-Bi). In other words the Au-Si resembles the highest value of nega-

tive heat of mixing followed by Au-Ge and is the only alloy to show anomalous surface behavior of the liquid phase. Although it is possible that the enhanced Au-Si enthalpy of mixing is an indication of stronger chemical bonding it is not clear why the $\sim 50\%$ difference should be sufficient to cause the observed differences in the surface properties.

Finally, the absence of Gibbs absorption at the surface might have been expected from the large negative enthalpy of mixing of Au-Ge relative to other alloys such as Au-Sn, Sn-Bi, etc. For example although the available lattice models for surface adsorption in metallic alloys (Guggenheim,⁴⁶ Strohl-King,⁴⁷ and Defay-Prigogine)⁴⁸ are not really quantitatively reliable they all predict that Gibbs absorption is repressed when the enthalpy of mixing is large and negative. In the present case application of the Guggenheim approximation using value of -21.5 kJ/mol for the enthalpy of mixing predicts a surface concentration of Ge of 0.36 at. % that is reasonably close to the bulk value of 0.28 at. %; however the predicted surface tension of ≈ 1240 mN/m is considerably larger than the measured value.

ACKNOWLEDGMENTS

This work has been supported by the U.S. Department of Energy through the grant No. DE-FG02-88-ER45379, S.M. is supported by the German Research Foundation through grant no. Me 3113/2-1, ChemMatCARS is principally supported by the National Science Foundation/Department of Energy under the grant No. CHE0087817. The Advanced Photon Source is supported by the U.S. Department of Energy, Basic Energy Sciences, Office of Science, under Contract no.: W-31-109-Eng-38.

-
- ¹O. M. Magnussen, B. M. Ocko, M. J. Regan, K. Penanen, P. S. Pershan, and M. Deutsch, *Phys. Rev. Lett.* **74**, 4444 (1995).
- ²M. J. Regan, E. H. Kawamoto, S. Lee, P. S. Pershan, N. Maskil, M. Deutsch, O. M. Magnussen, B. M. Ocko, and L. E. Berman, *Phys. Rev. Lett.* **75**, 2498 (1995).
- ³M. P. D'Evelyn and S. A. Rice, *J. Chem. Phys.* **78**, 5225 (1983).
- ⁴M. P. D'Evelyn and S. A. Rice, *Phys. Rev. Lett.* **47**, 1844 (1981).
- ⁵S. A. Rice, *Proc. Natl. Acad. Sci. U.S.A.* **84**, 4709 (1987).
- ⁶H. Tostmann, E. DiMasi, P. S. Pershan, B. M. Ocko, O. G. Shpyrko, and M. Deutsch, *Phys. Rev. B* **59**, 783 (1999).
- ⁷O. G. Shpyrko, P. Huber, A. Y. Grigoriev, P. S. Pershan, B. M. Ocko, H. Tostmann, and M. Deutsch, *Phys. Rev. B* **67**, 115405 (2003).
- ⁸O. G. Shpyrko, A. Y. Grigoriev, C. Steimer, P. S. Pershan, B. H. Lin, M. Meron, T. Graber, J. Gebhardt, B. M. Ocko, and M. Deutsch, *Phys. Rev. B* **70**, 224206 (2004).
- ⁹P. S. Pershan, S. E. Stoltz, O. G. Shpyrko, M. Deutsch, V. S. K. Balagurusamy, M. Meron, B. H. Lin, and R. Streitel, *Phys. Rev. B* **79**, 115417 (2009).
- ¹⁰E. DiMasi, H. Tostmann, O. G. Shpyrko, P. Huber, B. M. Ocko, P. S. Pershan, M. Deutsch, and L. E. Berman, *Phys. Rev. Lett.* **86**, 1538 (2001).
- ¹¹O. G. Shpyrko, A. Y. Grigoriev, R. Streitel, D. Pontoni, P. S. Pershan, M. Deutsch, B. M. Ocko, M. Meron, and B. H. Lin, *Phys. Rev. Lett.* **95**, 106103 (2005).
- ¹²H. Tostmann, E. DiMasi, P. S. Pershan, B. M. Ocko, O. G. Shpyrko, and M. Deutsch, *Phys. Rev. B* **61**, 7284 (2000).
- ¹³P. Huber, O. G. Shpyrko, P. S. Pershan, B. M. Ocko, E. DiMasi, and M. Deutsch, *Phys. Rev. Lett.* **89**, 035502 (2002).
- ¹⁴P. Huber, O. G. Shpyrko, P. S. Pershan, B. M. Ocko, E. DiMasi, and M. Deutsch, *Phys. Rev. B* **68**, 085409 (2003).
- ¹⁵B. Yang, D. Gidalevitz, D. X. Li, Z. Q. Huang, and S. A. Rice, *Proc. Natl. Acad. Sci. U.S.A.* **96**, 13009 (1999).
- ¹⁶B. Yang, D. X. Li, and S. A. Rice, *Phys. Rev. B* **67**, 212103 (2003).
- ¹⁷E. DiMasi, H. Tostmann, B. M. Ocko, P. S. Pershan, and M. Deutsch, *J. Phys. Chem. B* **103**, 9952 (1999).
- ¹⁸H. Tostmann, E. DiMasi, B. M. Ocko, M. Deutsch, and P. S. Pershan, *J. Non-Cryst. Solids* **250-252**, 182 (1999).
- ¹⁹O. G. Shpyrko, R. Streitel, V. S. K. Balagurusamy, A. Y. Grigoriev, M. Deutsch, B. M. Ocko, M. Meron, B. H. Lin, and P. S. Pershan, *Science* **313**, 77 (2006).
- ²⁰O. G. Shpyrko, R. Streitel, V. S. K. Balagurusamy, A. Y. Grigoriev, M. Deutsch, B. M. Ocko, M. Meron, B. H. Lin, and P. S. Pershan, *Phys. Rev. B* **76**, 245436 (2007).

- ²¹S. Mechler, S. E. Stoltz, E. Yahel, O. G. Shpyrko, S. Sellner, M. Meron, B. H. Lin, and P. S. Pershan, (to be published).
- ²²A. K. Green and E. Bauer, *J. Appl. Phys.* **47**, 1284 (1976).
- ²³A. K. Green and E. Bauer, *J. Appl. Phys.* **52**, 5098 (1981).
- ²⁴H. L. Gaigher and N. G. van der Berg, *Thin Solid Films* **68**, 373 (1980).
- ²⁵P. Ramachandrarao and T. R. Anantharaman, *Trans. Metall. Soc. AIME* **245**, 886 (1969).
- ²⁶W. Klement, R. H. Willens, and P. Duwez, *Nature (London)* **187**, 869 (1960).
- ²⁷H. Okamoto and T. B. Massalski, *Bull. Alloy Phase Diagrams* **5**, 627 (1984).
- ²⁸O. G. Shpyrko, M. Fukuto, P. S. Pershan, B. M. Ocko, I. Kuzmenko, T. Gog, and M. Deutsch, *Phys. Rev. B* **69**, 245423 (2004).
- ²⁹R. K. Heilmann, M. Fukuto, and P. S. Pershan, *Phys. Rev. B* **63**, 205405 (2001).
- ³⁰V. S. K. Balagurusamy, R. Streitl, O. G. Shpyrko, P. S. Pershan, M. Meron, and B. H. Lin, *Phys. Rev. B* **75**, 104209 (2007).
- ³¹P. S. Pershan, *Colloids Surf. A Physicochem. Eng. Asp.* **171**, 149 (2000).
- ³²P. S. Pershan, *J. Phys. Chem. B* **113**, 3639 (2009).
- ³³A. Wilson, *International Tables for X-Ray Crystallography* (Kluwer Academic, Dordrecht, 1992), Vol. C.
- ³⁴D. Cromer and J. Waber, (Kynoch Press, Birmingham/Kluwer Academic, Dordrecht, 1974).
- ³⁵S. Takeda, H. Fujii, Y. Kawakita, S. Tahara, S. Nakashima, S. Kohara, and M. Itou, *J. Alloys Compd.* **452**, 149 (2008).
- ³⁶R. Waghorne, V. Rivlin, and G. Williams, *J. Phys. F: Met. Phys.* **6**, 147 (1976).
- ³⁷O. G. Shpyrko, M. Fukuto, P. S. Pershan, B. M. Ocko, M. Deutsch, T. Gog, and I. Kuzmenko, The 8th International Conference on Surface X-Ray and Neutron Scattering, Germany 2004, (unpublished).
- ³⁸J. W. Gibbs, *The scientific papers of J. W. Gibbs*, edited by H. A. Bumstead and R. G. Van Name, (Longmans, Green, and Co., London, 1906), p. 219.
- ³⁹A. Takeuchi and A. Inoue, *Mater. Trans., JIM* **41**, 1372 (2000).
- ⁴⁰T. Iida and R. I. L. Guthrie, *The Physical Properties of Liquid Metals* (Clarendon Press, Oxford, UK, 1988).
- ⁴¹C. J. Aidinis, L. Bischoff, G. L. R. Mair, C. A. Londos, T. Ganetsos, and C. Akhmadaliev, *Microelectron. Eng.* **73-74**, 116 (2004).
- ⁴²C. J. Aidinis, G. L. R. Mair, L. Bischoff, C. A. Londos, C. Akhmadaliev, and T. Ganetsos, *Nucl. Instrum. Methods Phys. Res. B*, **222**, 627 (2004).
- ⁴³C. A. Croxton, *Statistical Mechanics of the Liquid Surface* (Wiley, New York, 1980).
- ⁴⁴H. W. Sheng, W. K. Luo, F. M. Alamgir, J. M. Bai, and E. Ma, *Nature (London)* **439**, 419 (2006).
- ⁴⁵D. B. Miracle, *Nature Mater.* **3**, 697 (2004).
- ⁴⁶E. A. Guggenheim, *Trans. Faraday Soc.* **41**, 150 (1945).
- ⁴⁷J. K. Strohl and T. S. King, *J. Catal.* **118**, 53 (1989).
- ⁴⁸R. Defay and I. Prigogine, *Trans. Faraday Soc.* **46**, 199 (1950).